J Mater Sci (2009) 44:1449–1455
DOI 10.1007/s10853-008-3169-x

Fabrication and finite element modeling of ellipsoidal macro-shells

K. B. Carlisle · V. Brito · G. M. Gladysz · W. Ricci · M. Koopman

Received: 29 February 2008 / Accepted: 5 December 2008 / Published online: 15 January 2009

Abstract Millimeter-sized composite spherical shells have long been used in syntactic foams for deep sea buoyancy applications. Recent advances in the understanding of particle settling behavior have revealed the enhanced packing factor of non-spherical shapes, especially of ellipsoidal geometries. In order to realize the packing advantage of ellipsoidal composite shells in syntactic foams, the potential mechanical property penalty as compared with spherical shells must be understood. The current investigation used linear elastic finite element models of isostatic compression to elucidate the mechanical difference between volumetrically identical spherical and ellipsoidal macro-shells. Experimental fabrication of glass-fiber/epoxy composite ellipsoidal macro-shells was also performed in order to verify the viability of the current industrial production process for non-spherical geometries. The relevant trends of increasing predicted stresses with increased deviation from sphericity are discussed, and their implications for syntactic foam properties and applications are discussed.

Introduction

Recent experimental and theoretical research into the effect of particle geometry on particle packing has determined that non-spherical geometries can possess greater space filling characteristics than can spherical particles. In particular, ellipsoids of revolution have exhibited random close packings nearly 12% higher than monosize spheres [1–3]. This is of direct interest to offshore and deep sea industries, where hollow spherical shells are currently used to lower density and increase the buoyant force of syntactic foams [4–7]. In these applications, microballoons are by far the most commonly used hollow shells, but there are significant industrial quantities of macroballoons being employed for certain applications. Current macroballoon production is based on a proprietary layer-by-layer coating process, similar in concept, if not scale, to the well-known core-template route of producing small hollow particles [8–10]. For composite macroballoons, particular fiber-to-reinforcement ratios are targeted depending on the specific fiber–matrix system. It is these macroballoons, of 4 to 150 mm in size, which are the perfect candidate for ellipsoidal geometries, both because their size is much easier to manipulate during evaluation and because their production process lends itself more readily to ellipsoid fabrication. If additional improvements in density and buoyant force characteristics could be made by employing higher packing fractions of ellipsoidal shells in offshore syntactic foams, this geometry could see significant application.

In order to determine the potential feasibility and applicability of ellipsoidal shells, research has been initiated to compare the strength of ellipsoidal shells to spherical shells, through the use of idealized finite element modeling. Furthermore, experimental fabrication of ellipsoidal macro-shells has been undertaken to determine the viability of fabricating ellipsoidal shells via the current industrial technique for producing millimeter-sized composite shells.

K. B. Carlisle (✉) · V. Brito · G. M. Gladysz · W. Ricci
Trelleborg Emerson and Cuming, Inc., 290 Forbes Blvd., Mansfield, MA 02048-1817, USA
e-mail: kipp.carlisle@trelleborg.com; kippcarlisle@gmail.com

M. Koopman
School of Engineering and Applied Sciences, Harvard University, 40 Oxford St, Cambridge, MA 02138, USA

Methods

Macro-shell fabrication

Generalized ellipsoidal cores of several sizes have been produced, using expanding copolymer microspheres and a closed mold. These ellipsoidal cores were then coated in micro-milled E-glass-fiber and epoxy through a proprietary coating process, by Trelleborg Emerson & Cuming, Inc. (Mansfield, MA, USA) to produce ellipsoidal macro-shells. The final composite walls contained fiber volume fractions tailored to achieve the desired shell strength and stiffness. The micro-milled E-glass-fiber used in this study had a low length-to-diameter ratio. Scanning electron microscopy (SEM), using a Philips 515 SEM (FEI Electron Optics, Eindhoven, Netherlands), was performed in secondary electron mode to evaluate the structure of the shells.

Macro-shell modeling

It is expected that ellipsoidal geometries will experience higher stresses when exposed to hydrostatic pressure, as compared with the stresses observed in spherical hollow shells, since their shape is no longer omni-symmetrical. In order to investigate the level of stress concentration, parametric, idealized finite element models were produced using ABAQUS 6.8-1. In this initial study, ellipsoidal shells of revolution were modeled and compared with a true spherical shell. To better facilitate comparison, the shell volume (6.78×10^{-4} m^3) and wall thickness (0.2 mm) were held constant across all models, and only the linear elastic regime was considered.

ABAQUS element choice was an 8-node, bi-quadratic, axisymmetric, quadrilateral element, used to include possible thick-shell effects. Some idealizations were made, with the major two being that the core has negligible effect on the system and that the shell wall was transversely isotropic, with the isotropic plane tangential to the shell. In the models, a local coordinate system was used wherein the 1-direction was the transverse direction and the 2–3 plane that of isotropy. Tables 1 and 2 provide the material properties of the composite's constituents and of the idealized composite, respectively, with the latter calculated through Halpin-Tsai equations [11] for transversely isotropic, random short fiber-reinforced composites.

Table 1 Composite constituent material properties

Material	Young's modulus, E (GPa)	Shear Modulus, G (GPa)	Poisson's ratio, ν	Volume fraction, V
E-glass	72.4	30	0.2	0.45
Epoxy	3.8	1.4	0.35	0.54

Table 2 Computed composite elastic constants

E_1 (GPa)	6.66	G_{12} (GPa)	3.37	ν_{12}	0.11
E_2 (GPa)	16.98	G_{13} (GPa)	3.37	ν_{13}	0.11
E_3 (GPa)	16.98	G_{23} (GPa)	6.12	ν_{23}	0.387

The imposition of hydrostatic pressure was chosen to replicate hydrostatic pressure testing based on ASTM D 3102-78 methods. In order to determine the maximum hydrostatic pressure to impose in the models, theoretical predictions for the probable actual elastic stability limit of an isotropic spherical shell were used (see Eq. 1).

$$P_{\mathrm{h}} = 0.365E\left(\frac{t}{R}\right)^2. \tag{1}$$

Equation 1 predicts the applied hydrostatic pressure (P_{h}) at the onset of elastic instability (buckling) in terms of the Young's modulus (E), wall thickness (t), and radius (R) of the shell [12].

For spherical shells of this R/t ratio, we know that elastic buckling is typically the failure mode, hence the use of Eq. 1. Given a spherical shell with the geometry given in Table 3, approximate bounds for the applied hydrostatic pressure were calculated by considering its planar and transverse moduli (16.98 and 6.66 GPa, respectively). An isotropic spherical shell with Young's modulus equal to the planar value calculated for the composite should buckle at an external hydrostatic pressure of 6.89 MPa, while the same shell having Young's modulus equal to the transverse modulus of these composites should buckle at 2.70 MPa applied hydrostatic pressure. Given that these are predicted bounds of the *probable actual elastic stability limit*—and the *theoretical* elastic stability limit should be significantly higher [12]—a maximum pressure of 7.0 MPa was applied in all *idealized* ABAQUS models. This pressure should produce stress states in the models near to those at failure, without either transcending the linear elastic regime or

Table 3 Input geometry for parametric ABAQUS models

$a = c$ (mm)	b (mm)	Aspect ratio, α (mm/mm)
7.114	4.268	0.6
6.840	4.617	0.675
6.757	4.730	0.7
6.604	4.953	0.75
6.463	5.171	0.8
6.334	5.384	0.85
6.214	5.593	0.9
6.103	5.798	0.95
6	6	1

inducing elastic buckling. The relative stress states can then be evaluated across shell geometry.

As per established conventions [1], the ellipsoidal shells' geometry was specified by the major and minor radii lengths (a, b and c, respectively). For shells of revolution, two radii will be equal ($a = c$), with the third being less than the others ($a > b$) for oblate ellipsoids. The spherical case is defined by all radii of equal length. Aspect ratio (α) was used to represent the relative sphericity of the shells being modeled, and is defined in Eq. 2, below.

$$\alpha = \frac{b}{a}. \tag{2}$$

The aspect ratio presentation method for the geometric inputs listed in Table 3 allows for easy comparison with other scholarly work on particle packing [1], allowing for increased design utility.

Results and discussion

Experimental observations

Fabrication of ellipsoidal macro-shells of a generalized nature ($a \neq b \neq c$) was performed, and the resulting ellipsoids are shown in Fig. 1a. Comparing these ellipsoids to the spherical macro-shells shown in Fig. 1b, the ellipsoids were observed to be of comparable quality to the commercial spherical macro-shells. Thus, the core-template route demonstrated its ability to generate ellipsoids of a variety of sizes with acceptable surface smoothness and geometric regularity. However, more quantitative examination through SEM was required to verify the uniformity of the microstructure. Of special concern was the possibility of wall thickness variations due to the changing curvature of the shells. Figure 2a–d shows a series of SEM

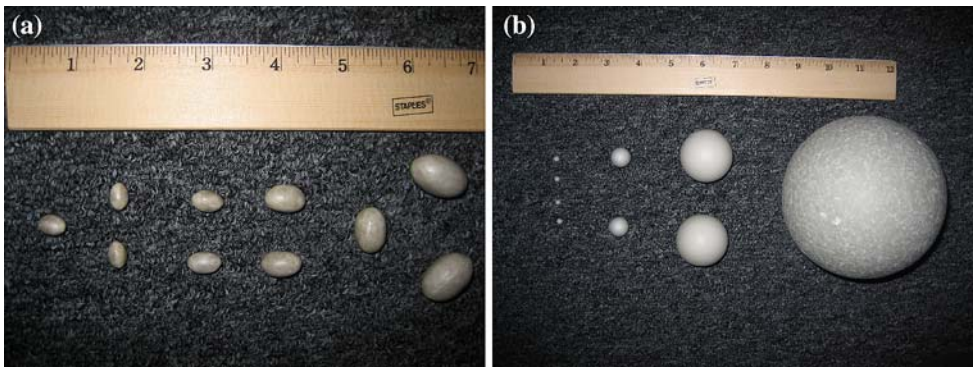

Fig. 1 **a** Ellipsoidal glass-fiber/epoxy macro-shells produced using molded cores. **b** Commercially produced spherical macro-shells

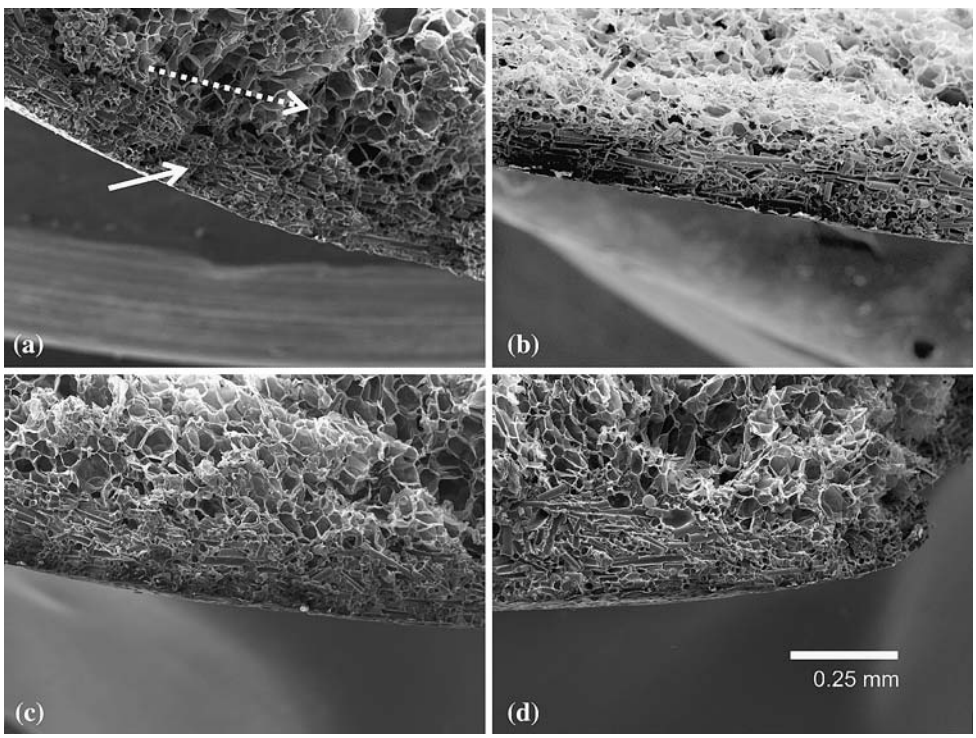

Fig. 2 SEM micrographs of broken ellipsoidal macro-shell. Micrographs taken from **a** minor axis, **b** center of major axis, **c** near tip on major axis, **d** at tip on major axis. *Dashed arrow* in (**a**) indicates core, *solid arrow* denotes fiber-reinforced shell wall. No significant wall thickness variations were observed. Fiber-reinforced epoxy structure appears uniform and void-free

micrographs taken from different regions along the shell wall, with the fiber-reinforced plastic (FRP) wall and core visible in each image. The average wall thickness was estimated to be 0.2 mm, with little or no variation with location along the shell. The FRP wall material consisted of a continuous coating with near-random fiber orientation in the hoop direction. Therefore the planar isotropy assumptions in the calculation of input properties for the models (Tables 1 and 2) were reasonable. The samples were also largely free from major structural defects, i.e., voids. Thus, it was concluded that the current core-template coating process may be adapted to produce ellipsoidal macro-shell geometries.

Modeling

While the level of idealization precluded predicting failure stresses in experimental samples, the simulation results were sufficient to illustrate the key features of the work. The primary focus was to examine the stress concentration effect on the von Mises stresses ($\sigma_{\text{von Mises}}$) caused by deviations from sphericity, under an applied hydrostatic pressure. While the choice of $\sigma_{\text{von Mises}}$ for this comparison may seem unusual in relation to other studies [13], especially for the linear elastic regime, it has some justification. The initial inclination would be to examine the first principle stress distributions; however,

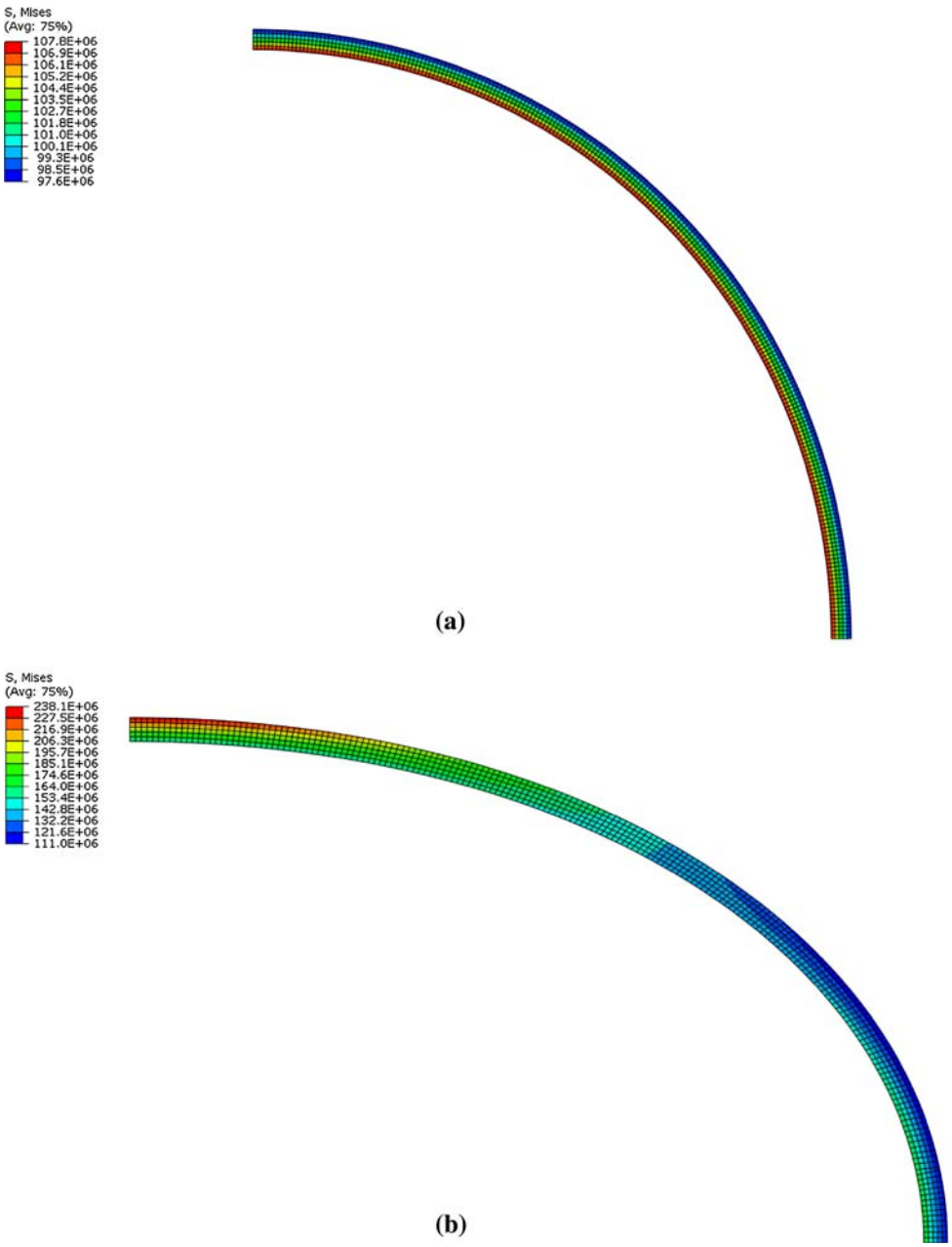

Fig. 3 $\sigma_{\text{von Mises}}$ distribution for volumetrically identical macro-shells with **a** spherical ($\alpha = 1$) and **b** very ellipsoidal ($\alpha = 0.675$) aspect ratios. Predicted effective stresses are 221% higher at a 32.5% deviation from sphericity. Note the change in the character of the stress distribution from uniform to increasingly more localized concentrations. Stresses units are Pascals (Pa)

the corresponding Rankine failure criterion has a main weakness in that it incorrectly predicts plastic flow under hydrostatic pressures [13]. Thus, first principle stresses and the Rankine criteria would be a poor choice for later study. $\sigma_{\text{von Mises}}$ were therefore the logical choices, as they represent the effective stress in the material and are based on distortion energy. In the corresponding maximum distortion energy failure criteria, complex stress states are easily handled, including hydrostatic pressures [14, 15]. An analysis of this sort could easily overestimate the strength of the ellipsoidal shells, as it fails to account for local tensile stresses from bending under hydrostatic pressure. Therefore the hoop direction stresses (σ_{hoop}) were also investigated.

As can be seen in Fig. 3, which shows $\sigma_{\text{von Mises}}$ distributions for a spherical and a significantly ellipsoidal macroshell, the stress levels increased dramatically as the aspect ratio deviated further from unity. Additionally, we observed that the distribution changed character after a minimum deviation from sphericity. For more spherical ellipsoidal shells, the stress distribution was uniform and of only slightly higher magnitude than that for a spherical shell (e.g., Fig. 3a). In Fig. 3b, the distribution shifted to create a concentrated area of high stress along the minor radius, with stresses increasing non-linearly with increased curvature. Models with aspect ratios between those illustrated in Fig. 3a, b followed similar trends. This follows intuitively from the role of curvature in fracture mechanics [14, 15].

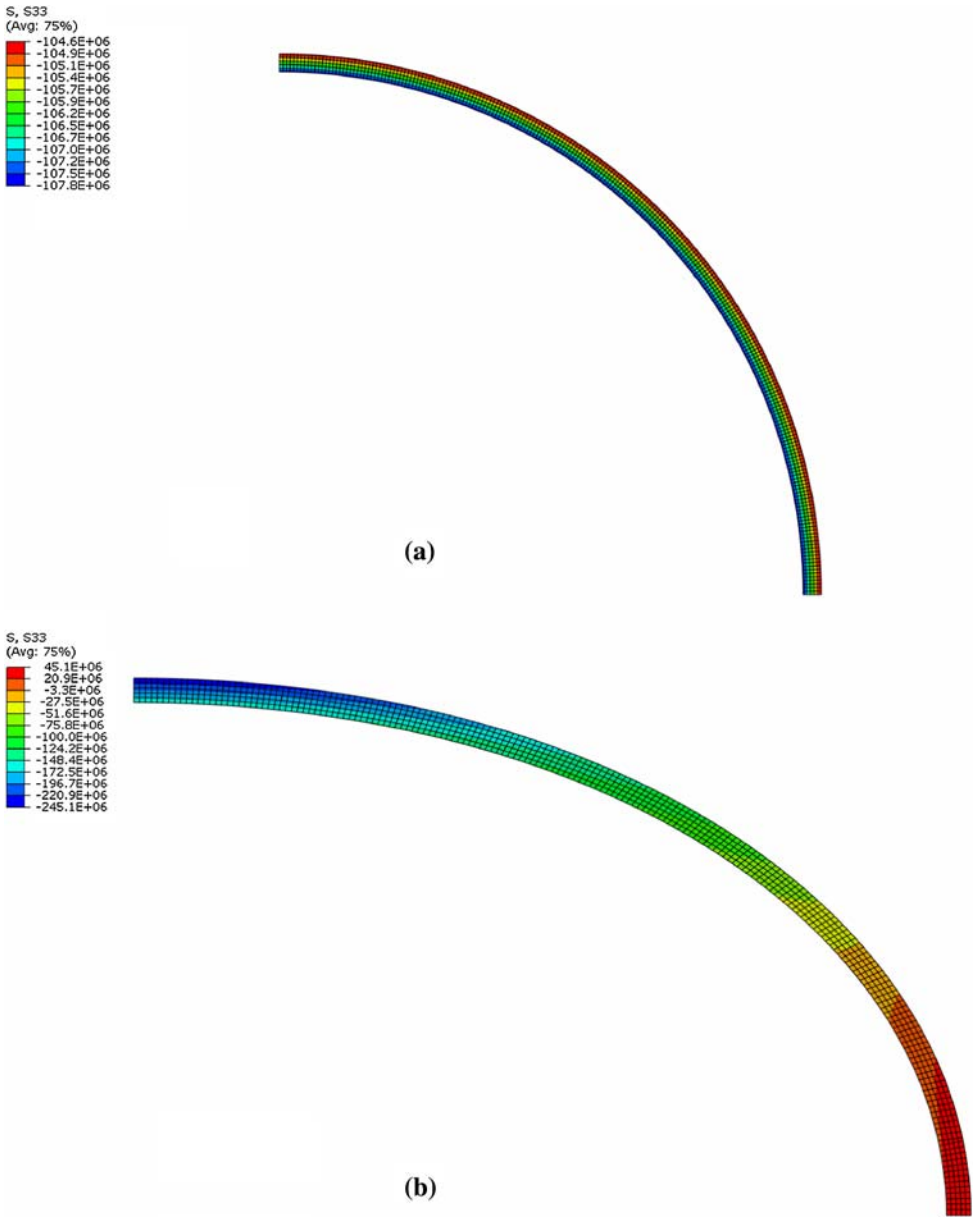

Fig. 4 σ_{hoop} distribution for volumetrically identical macroshells with **a** spherical ($\alpha = 1$) and **b** very ellipsoidal ($\alpha = 0.675$) aspect ratios. σ_{hoop} values are uniform and compressive in the spherical case, but have changed to much more compressive along the minor axis and tensile along the major axis in the ellipsoidal model. Tensile σ_{hoop} values were observed for all ellipsoids of $\alpha \leq 0.7$. Stresses units are Pascals (Pa)

For non-spherical shells, it is possible that the geometry could lead to stress localizations and local tensile stresses due to bending. In this case, the eventual failure of the shell might be a tensile failure of the shell wall instead of buckling. In order to investigate this possibility, the σ_{hoop} distributions were examined for each of the models, and representative distributions are presented in Fig. 4. For $\alpha \leq 0.7$, it was found that local tensile stresses do indeed arise under the applied hydrostatic loading (Fig. 4b), but their magnitude for $0.675 \leq \alpha \leq 1$ was at most 45.1 MPa. This is not expected to cause tensile fracture of the composite.

We have based the modeling on the theory that buckling is the primary failure mode of spherical macro-shells. In order to evaluate the stress concentration of the ellipsoidal geometries, all models employed an applied hydrostatic pressure near that at the probable actual elastic instability limit of the spherical macro-shell [12]. The issue of buckling the ellipsoids, especially those of low aspect ratio, under this load must be addressed. For ABAQUS implicit simulations of macro-shells of $\alpha \leq 0.65$, complete solutions were not obtainable. Only a portion of the full hydrostatic pressure was able to be applied, and latter increments of the solver run diverged, with at least one negative eigenvalue. This is indicative of a buckling scenario. To corroborate this, a quasi-static simulation was performed using the ABAQUS explicit solver for $\alpha = 0.6$. The $\sigma_{\text{von Mises}}$ distributions for the time increments corresponding (approximately) to the last converged increment and to the first diverging increment of the implicit solution are shown in Fig. 5a, b, respectively. It was immediately apparent that elastic buckling has occurred. The most

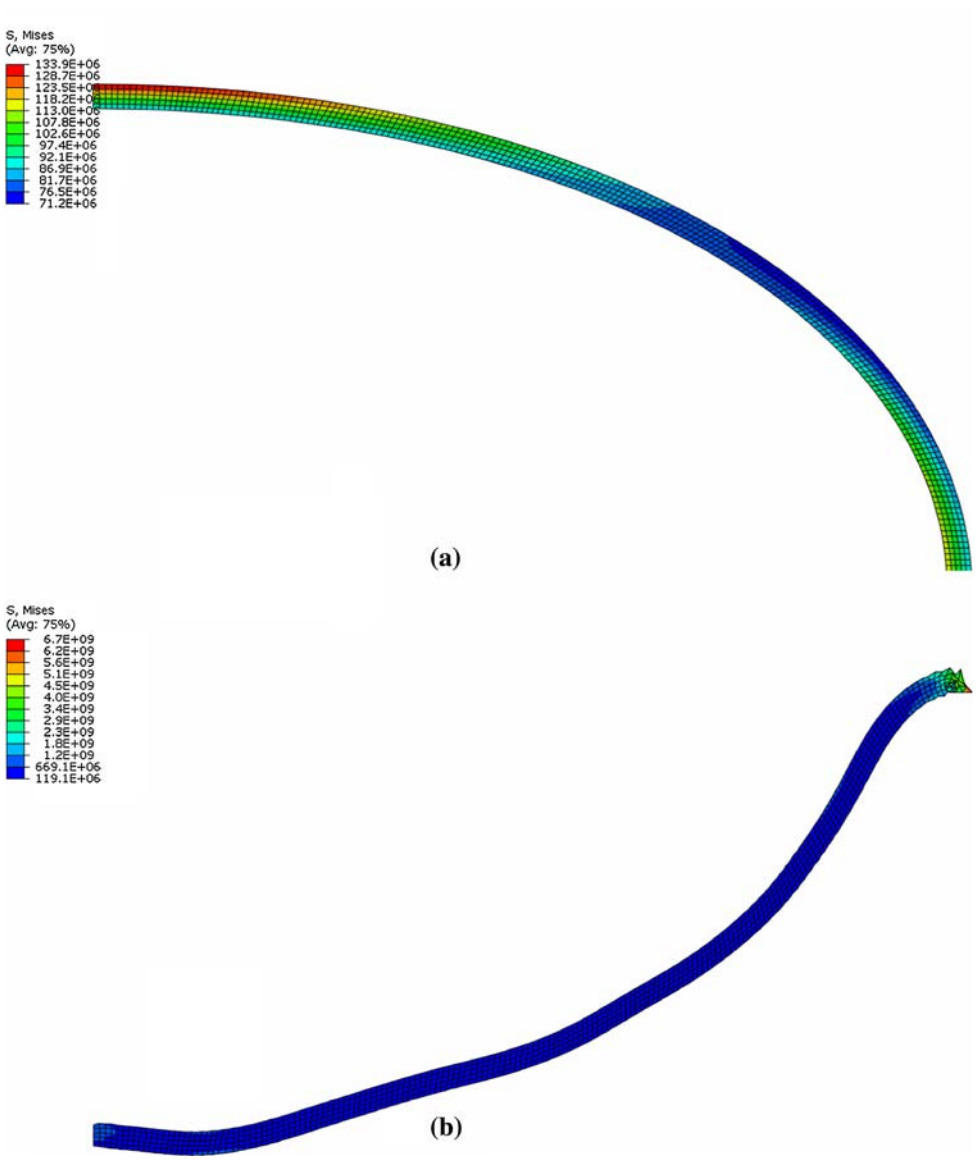

Fig. 5 Explicit FEA solver's prediction of $\sigma_{\text{von Mises}}$ distribution immediately **a** before and **b** after elastic buckling for ellipsoid of $\alpha = 0.6$. Loads and stresses in (**a**) correspond to those in the last converging time step of implicit solution, indicating that negative eigenvalue detection in next increment did indeed indicate buckling. Stresses units are Pascals (Pa)

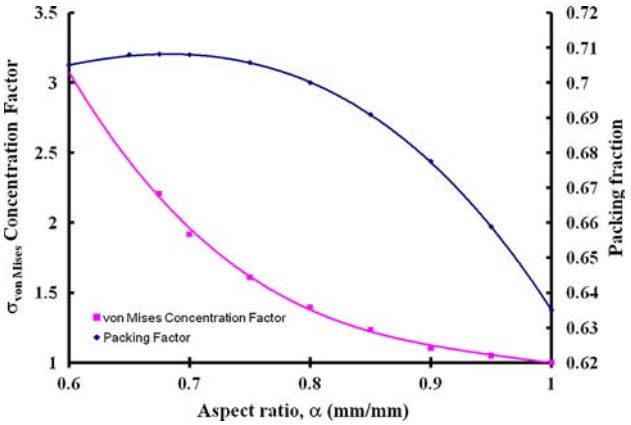

Fig. 6 Predicted $\sigma_{\text{von Mises}}$ concentration factor and packing fraction as functions of aspect ratio for oblate ellipsoids. Aspect ratios between 0.85 and 1.0 provide up to 9% increases in packing factor at up to a 23% increase in $\sigma_{\text{von Mises}}$. Note that elastic buckling was predicted for $\alpha < 0.675$. Packing data after ref. [1]

important consequence of predicting buckling for the lower aspect ratios is the implication that the models of $\alpha > 0.65$ did not exceed the elastic instability limit under the 7 MPa applied hydrostatic pressure. This provides significant validation to the previous stress concentration discussion.

Figure 6 displays the results from parametric models of other intermediate aspect ratios, giving maximum $\sigma_{\text{von Mises}}$ concentration factor as a function of aspect ratio plotted along with maximum packing fractions. All ellipsoidal models may thus be simultaneously compared with the spherical case, for which both stress concentration factor and aspect ratio are unity. Immediately apparent was the prediction of a power–law dependence of predicted effective stress state on shell aspect ratio. Since the effective stresses shown are within the linear elastic regime, comparisons to failure models are of limited use, but the simplified models illustrated the point that the failure stress of the material will be reached at lower hydrostatic pressure loads with less spherical geometries. This is due entirely to the stress concentration at the high radius of curvature regions.

Figure 6 also illustrates the potential of balancing desired shell strength with the capacity to create lower density syntactic foams. The secondary axis in Fig. 6, packing fraction, correlated the current strength simulation results to research on the packing efficiency of oblate ellipsoids [1]. Our findings indicated that ellipsoids of aspect ratios between 0.85 and 0.95 incur a 5–23% strength penalty relative to spheres while simultaneously enhancing the maximum packing density by 3.8–8.8% [1, 3]. This result indicates that carefully selected ellipsoidal shell geometries, with packing fractions equivalent to some binary sphere blends [1, 3], may be used to further decrease the density of syntactic foam composites without excessive strength penalty.

Conclusions

This initial study has shown that ellipsoidal macro-shells can be manufactured using current industrial technology. Additionally, the extent of the stress concentration when using ellipsoidal shells versus spherical shells was investigated, and preliminary models suggested that ellipsoidal geometries may be carefully selected to achieve minimal strength penalties. As expected, all ellipsoidal geometries had increased stresses versus spherical macro-shells, with the increase in effective stress obeying a power–law relationship with aspect ratio. It was found that oblate ellipsoids that deviate beyond 35% from sphericity will experience elastic instability at increasingly lower applied hydrostatic pressures, whereas oblate ellipsoids of aspect ratios >0.85% offered only minimal disadvantages in performance. Thus, ellipsoidal macro-shells of the proper aspect ratio may be a viable reinforcement for low density, high-strength syntactic foams. Further study of ellipsoidal macro-shells will focus on extending the current investigation to ellipsoids of prolate and generalized geometries, and to experimentally verify ellipsoidal macro-shell packing fractions and hydrostatic strengths. Additionally, ABAQUS models may be refined to reflect the actual failure properties of the FRP composite from which the macro-shells were fabricated.

References

1. Donev A, Cisse I, Sachs D, Variano E, Stillinger F, Connelley R, Torquato S, Chaikin P (2004) Science 303:990
2. Delaney G, Weaire D, Hutzler S, Murphy S (2005) Philos Mag Lett 85:89
3. McGeary (1961) J Am Ceram Soc 44:413
4. DeRuntz J, Hoffman O (1969) J Appl Mech 36:551
5. Okuno K, Woodhams R (1974) J Cell Plast 10:237
6. Whitaker T (1980) In: Proceedings of 16th joint propulsion conference, Hartford, CT
7. Gupta N, Woldesenbet E (2003) Compos Struct 61:311
8. Wilcox D, Berg M (1995) Mater Res Soc Symp Proc 372:3
9. Bourlinos A, Boukos N, Petridis D (2002) Adv Mater 14:21
10. Kim M, Bon Yoon S, Sohn K, Kim J, Shin C, Hyeon T, Yu J (2003) Microporous Mesoporous Mater 63:1
11. Mallick PK (ed) (1997) Composites engineering handbook. Marcel Dekker, New York
12. Young W, Budynas R (2002) Roark's formulas for stress and strain. McGraw Hill, New York, p 585, 597, 737
13. Carlisle K, Lewis M, Chawla K, Koopman M, Gladysz M (2007) Acta Mater 55:2301
14. Meyers M, Chawla K (1999) Mechanical behavior of materials. Prentice Hall, Upper Saddle River
15. Hertzberg R (1996) Deformation and fracture mechanics of engineering materials. Wiley, New York